kcal/mol,[50] which confers a certain consistency to our results.

D. Concluding Remarks. The unimolecular reactivities for each H_2PN isomer involve 1,2-hydrogen shifts.[51] We did not study the corresponding barrier heights, but theoretical results on 1,2-hydrogen shifts with breaking of a NH bond are available, for instance

$$H_2C{=}NH \rightarrow H_3C{-}N:$$

singlet, $\Delta E = +85$ kcal/mol; no barrier[22]

$$H_2C{=}NH \rightarrow H_3C{-}N:$$

triplet, $\Delta E = -18$ kcal/mol; $\Delta E^{\ddagger} = 35$ kcal/mol[22]

$$HN{=}NH \rightarrow H_2N{-}N:$$

singlet, $\Delta E = +26$ kcal/mol; $\Delta E^{\ddagger} = 83$ kcal/mol[10]

These results together with others concerning breaking of CH bonds such as

$$HC{\equiv}CH \rightarrow H_2C{=}C:$$

singlet, $\Delta E = +40$ kcal/mol; $\Delta E^{\ddagger} = 48$ kcal/mol[52]

$$HC{\equiv}CH \rightarrow H_2C{=}C:$$

triplet, $\Delta E = +1$ kcal/mol; $\Delta E^{\ddagger} = 70$ kcal/mol[53]

$$H_3C{-}CH \rightarrow H_2C{-}CH_2$$

triplet, $\Delta E = -2$ kcal/mol; $\Delta E^{\ddagger} = 53$ kcal/mol[54]

tend to suggest significant energy barriers for all the 1,2-hydrogen shifts that are possible in our singlet and triplet H_2PN isomers. However, one must bear in mind that bimolecular hydrogen exchanges may require lower barriers, for instance, only 4 kcal/mol for the aminonitrene → *trans*-diimide reaction according to STO-3G calculations by Kemper and Buck.[55] On the other hand, it is obvious that a singlet >P–N framework prefers polymolecular reactivity and should give, for instance, stable cyclotriphosphazene.

This work, which deals only with the static description of the singlet and triplet H_2PN potential energy surfaces, led to the following main results: (1) $H_2P{-}N$ has a singlet ground state but is the least stable structure despite the high multiplicity of its PN bond; (2) $H_2N{-}P$ has a triplet ground state; (3) cis and trans singlet HP=NH and triplet $H_2N{-}P$ are the most stable isomers and are nearly degenerate in energy.

Acknowledgment. I thank Dr. R. Wolf and Professor J. Barrans for helpful discussions and suggestions concerning the chemical aspects of this work. I am also grateful to Drs. J. P. Daudey and J. P. Malrieu for their theoretical and computational aid.

Registry No. *cis*-**1**, 58734-29-5; *trans*-**1**, 58734-30-8; **2**, 83486-79-7; **3**, 83486-80-0.

(51) For reviews on 1,2-hydrogen shifts, see: Dykstra, C. E. *Annu. Rev. Phys. Chem.* **1981**, *32*, 25. Schaefer III, H. F. *Acc. Chem. Res.* **1979**, *12*, 288.

(52) Osamura, Y.; Schaefer, H. F.; Gray, S. K.; Miller, W. H. *J. Am. Chem. Soc.* **1981**, *103*, 1904.

(53) Conrad, M. P.; Schaefer, H. F. *J. Am. Chem. Soc.* **1978**, *100*, 7820.

(54) Harding, L. B. *J. Am. Chem. Soc.* **1981**, *103*, 7469.

(55) Kemper, M. J. H.; Buck, H. M. *Can. J. Chem.* **1981**, *59*, 3044.

Crystal Structure of Dehydrated Sr-Exchanged Zeolite A. Absence of Near-Zero-Coordinate Sr^{2+}. Presence of Al Complex

Joseph J. Pluth and Joseph V. Smith*

Contribution from the Department of the Geophysical Sciences, The University of Chicago, Chicago, Illinois 60637. *Received March 15, 1982*

Abstract: Single crystals of Linde zeolite 4A were ion exchanged with a mixed solution of $Sr(ClO_4)_2$ and $Sr(OH)_2$ at room temperature to take advantage of stability under basic conditions and clean exchange in chlorate solution. Electron microprobe analyses revealed only insignificant amounts of Na and K. X-ray diffraction data for a crystal dehydrated at 350 °C, and another at 500 °C, were refined with space group $Fm\bar{3}c$ ($a = 24.68$ Å). Only the (111) diffraction violated the space-group extinctions. The mean T–O distances (1.599 and 1.730 Å) correspond to alternation of tetrahedra populated by Si and $\sim Al_{0.9}Si_{0.1}$, in conformity with earlier structural analyses and in complete disagreement with recent speculations of a 3:1 ordering model. All Sr atoms lie near the center of 6-rings, in disagreement with an earlier structure determination of an unanalyzed crystal for which one Sr was placed in an 8-ring; perhaps this latter position actually corresponds to K scavenged during ion exchange. Approximately four-fifths of the Sr atoms (Sr(1), 4.5 atoms per pseudocell) project into the large cage, and one-fifth (Sr(2), 1.2 atoms) project into the sodalite unit. Both types are bonded to three O(3), respectively at about 2.4 and 2.5 Å. Electron density at the center of the sodalite unit and on the triad axes is attributed to Al in a tetrahedron of oxygen species, disordered in two orientations. Such electron density is found in most varieties ion exchanged with divalent cations.

The concept of zero-coordination[1] for monovalent cations was disproven by accurate structural determination of dehydrated zeolite A[2] and the dehydrated K-exchanged variety.[3] The present structure determination of the dehydrated Sr-exchanged variety provides a test of the claim for near-zero-coordination of divalent cations that is apparently supported by structure determinations[4,5] of crystals of zeolite A dehydrated after exchange with solutions containing Cd^{2+}, Eu^{2+}, Ca^{2+}, and Sr^{2+}. In the present study, electron microprobe analysis of exchanged crystals demonstrates problems caused by scavenging of trace impurities during ion exchange, but such problems were not considered in ref 4 and 5. Weak electron density in the sodalite unit of the present structure is ascribed to a spatially disordered, occluded tetrahedral complex produced during ion exchange, and not occluded during initial crystallization.[6]

(1) Firor, R. L.; Seff, K. *J. Am. Chem. Soc.* **1976**, *98*, 5031–5033.

(2) Pluth, J. J.; Smith, J. V. *J. Am. Chem. Soc.* **1980**, *102*, 4704–4708.

(3) Pluth, J. J.; Smith, J. V. *J. Phys. Chem.* **1979**, *83*, 741–749.

(4) (a) Firor, R. L.; Seff, K. *J. Am. Chem. Soc.* **1977**, *99*, 7059–7061. (b) *Ibid.* **1978**, *100*, 978–980. (c) *Ibid.* **1978**, *100*, 3091–3096.

(5) McCusker, L. B.; Seff, K. *J. Am. Chem. Soc.* **1978**, *100*, 5052–5057.

0002-7863/82/1504-6977$01.25/0

Table I. X-ray Diffraction Data and Structure Refinement

	PSa	PSb	FS
exchange soln, T	equal volumes of 0.5 M $Sr(ClO_4)_2$ and saturated $Sr(OH)_2$ at ~25 °C		saturated $Sr(OH)_2$ at ~25 °C
dehydration temp, °C	350	500	350
cryst diameter, μm	72	78	80
space group	$Fm\bar{3}c$	$Fm\bar{3}c$	$Pm3m$
wavelength, Å	1.5418	1.5418	0.71069
monochromator	graphite	graphite	graphite
cell dimensions, Å	24.674 (1)	24.687 (1)	12.316 (2)
diffractometer	Picker FACS-1	Picker FACS-1	Syntex $P2_1$
orientation	2° from a	2° from a	?
scan technique	fixed θ–2θ	fixed θ–2θ	fixed θ–2θ
speed, deg/min	1	1	1
range, deg	1.3–1.9	1.3–1.9	1.6
background	fixed 40 s	fixed 80 s	variable scan/bkgd = 1
total intensities measd	3449 (1876)[a]	3458 (1869)[a]	1782
unique data set	596 (376)[a]	594 (384)[a]	891
significant data set	494 (371)[a] 2σ	408 (346)[a] 2σ	307
$(\sin\theta)/\lambda_{max}$	0.59	0.59	0.81
absorptn coeff	92.9	92.9	
absorptn correctn	yes	yes	no
R	0.038 (0.036)[a]	0.038 (0.035)[a]	0.111
weighted R	0.045 (0.044)[a]	0.039 (0.039)[a]	0.096
S	4.19 (4.74)[a]	2.77 (2.94)[a]	4.54

[a] Numbers in parentheses refer to pseudostructure.

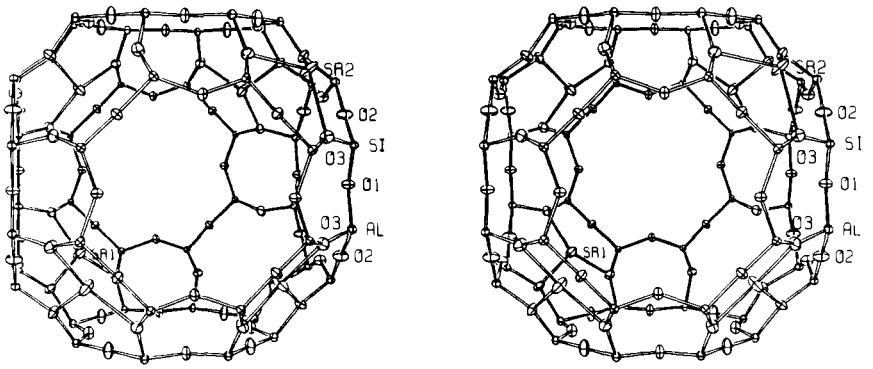

Figure 1. Stereoplot of large cage with representative positions for Sr atoms. Ellipsoids at 30% probability level.

Experimental Section

Specimen Preparation. Crystals of zeolite 4A (Na-A) were prepared by a modification of Charnell's method[7] including a second crystallization using seed crystals from the first synthesis. Thirty crystals were sealed in a vial filled with water saturated with $Sr(OH)_2$ (Alfa 72115), and the solution (pH ~12) was changed twice during a 2-week period at room temperature. Semiquantitative electron microprobe analysis showed significant Na and K in the exchanged crystals, and it was concluded that a trace impurity of K was being scavenged from the saturated solution which contains only 1.74 wt % $Sr(OH)_2$ at 20 °C.

An attempt was then made to use 0.5 M $Sr(ClO_4)_2$ solution (Alfa 72115) with pH ~6.7 to suppress any possible K contamination. Although electron microprobe analysis showed complete exchange of Na by Sr, not by K, after 17 days, X-ray oscillation photographs showed only poor crystallinity. To take advantage of stability under basic conditions coupled with clean exchange in chlorate solution, we then exchanged crystals in an equal-volume mixture of 0.5 M $Sr(ClO_4)_2$ and saturated $Sr(OH)_2$ solutions. Exchange was incomplete after 14 days at room temperature, but electron microprobe analysis of crystals exchanged for a further 41 days detected only Al, Si, and Sr except for traces (<0.2 wt %) of Na_2O and K_2O in some but not all crystals. Quantitative spectrometer analyses were made at 15 Kv, sample current ~10 nA, spot diameter 16 μm, with the MAGIC correction procedure and the following standards: Sr, synthetic $SrAl_2Si_2O_8$; Na, Al, Si, and Ca, synthetic plagioclase An_{70}; K, asbestos microcline. A total of 20 analyses on different spots of two crystals used for collection of X-ray data gave the following ranges when calculated to 48 oxygens: Sr, 5.2–5.5; Al, 11.5–11.8; Si, 12.4–12.7 atoms. The Al and Si analyses confirm the earlier evidence[2,3] for an Al/Si ratio less than unity. The Sr analyses are too low for charge balance with Al (5.2–5.5 vs. ~5.8–5.9), but this is believed to result at least mainly from an incorrect algorithm for matrix correction of the Lα spectral line for Sr. Correction procedures are based mainly on K spectra, and may not apply accurately to L spectra. The population refinements (see later) indicate a higher Sr content (Table II; 5.7 Sr per 48 oxygens), which is closer to the value of 5.9 required for charge balance with Al.

Two cubes were lodged in silica capillaries and dehydrated (under 10^{-5} torr), the first (PSa) at 350 °C for 50 h and the second (PSb) at 500 °C for 66 h. After being sealed under high vacuum at temperature, the samples were cooled slowly to room temperature.

X-ray Data Collection. Diffraction data for both cubes were collected on the same Picker FACS-1 diffractometer but with different sources of Cu Kα radiation: PSa, Rigaku 12-kW rotating-anode generator, 40 kV, 190 mA, 0.5 × 0.5 mm focal spot; PSb, sealed X-ray tube, constant potential 30 kV, 20 ma, 0.4 × 0.4 mm focal spot. The 5-fold increase of integrated intensity for PSa allowed an increase of 20% in observed diffractions (Table I) and a doubling of those for the superstructure. The significant data set for both cubes is larger than that obtained by Firor and Seff[4c] for a crystal (FS) exchanged with $Sr(OH)_2$ solution and dehydrated at 350 °C. The cell dimensions for PSa and PSb were obtained by least-squares refinement using 2θ angles for 15 Friedel pairs ($44° < 2\theta < 70°$) and weighted wavelengths for Cu Kα. A Gaussian integration formula for the absorption correction gave maximum and minimum transmission factors of 0.49–0.60. Diffraction intensities obey cubic symmetry and were averaged; Lorentz and polarization factors were applied and errors calculated as in ref 2. All PS diffractions obey $Fm\bar{3}c$ at the 3σ detection level except for 111 with intensity 453 ± 37 (PSa) and 198 ± 21 (PSb). This weak diffraction is attributed to the extraframework species.

Structure Refinement. Least-squares refinements (labeled f) of the PS data sets converged rapidly for the 24-Å supercell in $Fm\bar{3}c$ in spite of correlation coefficients as high as 0.9. Starting parameters for framework atoms were taken from dNa-A (dehydrated Na-A),[2] and two sites were used for Sr displaced either into the supercage (Sr(1)) or the sodalite unit (Sr(2)) from the center of the 6-ring (Figure 1). There was no significant electron density near the plane of the 8-ring, and site Sr(3) from

(6) Basler, W. D.; Miawald, W. *J. Phys. Chem.* **1979**, *83*, 2148–2151.
(7) Charnell, J. F. *J. Cryst. Growth* **1971**, *8*, 291–294.

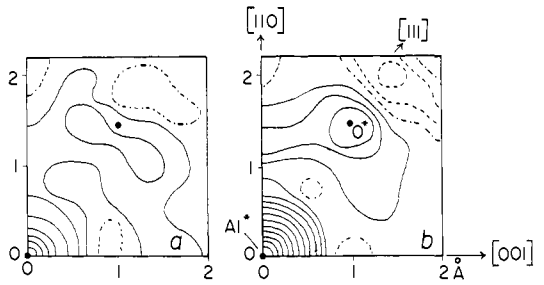

Figure 2. Residual electron density in (110) plane passing through the origin for refinements PSfa and PSfb. Zero and negative contours, dot-dash and dash, respectively. Contours at 0.2 e/Å^3, except for origin peak with 0.4 e/Å^3.

ref 1 was ignored. However, residual electron density was found at the center of the sodalite unit (coordinates 0,0,0; sharp spherical peak 2.9 e/Å^3, PSa; 4.8 e/Å^3, PSb) and at eight symmetry-related positions on the body diagonals (±0.04, ±0.04, ±0.04; irregular peak, 0.5 e/Å^3, PSa, 0.7 e/Å^3, PSb). The (110) planar section (Figure 2) is similar for both crystals when account is taken of experimental error, and the residuals are generally higher for PSb than PSa. Because the distance between the sharp and irregular peaks is about 1.7 ± 0.2 Å, the electron density was modeled by two fractional AlO_4 tetrahedra, each of which (Figure 3) accounts for half of the origin peak and four out of the eight irregular peaks. Averaging of the two tetrahedral orientations generates the cubic array of eight irregular peaks arranged symmetrically about the origin peak. Least-squares refinement with Al* at the origin for PSb yielded a reduction of conventional R and R_w from 0.045 and 0.048 to 0.039 and 0.042. The largest residual peak in a difference Fourier (0.72 e/Å^3 at $x = y = z = 0.038$) was then ascribed to oxygen O*. Least-squares refinements of framework atoms plus the population factor (Al*, O*) were unstable, but convergence was achieved (Table II) after fixing the Al*–O* distance at 1.74 Å. Only slight decrease occurred in R (0.038) and R_w (0.039). A similar least-square refinement was then obtained for PSa (Table II). For a comparison with the refinement by Firor and Seff[4c] in the 12-Å *Pm3m* pseudocell, refinements of the PSa and PSb data were then made (Table II, labeled p).

The least-squares refinements used atomic scattering factors and anomalous scattering corrections for Si^{2+}, Al^+, O^-, and Sr^{2+} from "International Tables for X-ray Crystallography", with interpolation between factors for Si and Si^{4+} and for Al and Al^{3+}. Refinements in *Pm3m* used $(Si^{2+} + Al^+)/2$. The largest peak in the final difference Fourier map is ~1.0 e/Å^3 at $x = y = z = 0.13$ for PSfa and ~0.5 eÅ^3 at $x = y = z = 0.14$ for PSfb.

Discussion

Framework. The dimensions of the aluminosilicate framework are equal within experimental error for refinements PSfa and PSfb, and the overall mean T–O distances of 1.599 and 1.730 Å are similar to those of 1.596 and 1.731 Å for dNa-A[3] and 1.602 and 1.736 Å for dK-A.[2] This confirms the earlier conclusion that Si and Al atoms show strong alternation on the tetrahedral nodes of zeolite A,[8] as is now reaffirmed by reinterpretation[9] of various NMR, electron-microscopic, and neutron-diffraction data.

As demonstrated for many aluminosilicates, especially for feldspar minerals (e.g., ref 10), the details of chemical bonding can affect the mean T–O distance in a TO_4 tetrahedron by ~0.01 Å, and estimation of Al content from a linear relation between Si–O near 1.60 Å to Al–O near 1.74–1.75 Å is uncertain to about 5%. The present distances of 1.599 and 1.730 Å indicate essentially complete occupancy of the first tetrahedron by Si, and somewhat less than full occupancy (~90%) of the second tetrahedron by Al. This is consistent with the electron microprobe evidence for a deficiency of Al from the ideal Si/Al ratio of unity. Whereas the ranges of O–T–O angles for dNa-A (106.0–112.3°) and dK-A (106.9–112.6°) indicate moderate distortion of the tetrahedra, the range for dSr-A (103.5–115.1°) indicates strong distortion, as befits interaction with a divalent cation with higher ionic potential. In all three structures, corresponding angles from SiO_4 and AlO_4 tetrahedra are closely similar, and in dSr-A the maximum difference is only 0.5 ± 0.5°. The T–O–T angles in dSr-A (141.2°, 177.7°, 147.0°) are different from those in dNa-A (142.2°, 164.7°, 144.8°) and dK-A (128.5°, 177.2°, 151.9°). A detailed analysis of the topochemical controls on framework geometry is being developed.

Strontium Positions. The present refinements for analyzed crystals show Sr positions only near the center of the 6-rings and not near the 8-rings. It is suggested that the Sr(3) position for the unanalyzed crystal in ref 4c was assigned incorrectly to Sr and may actually represent a small amount of potassium impurity. The positional and thermal parameters for position Sr(3) are poorly defined (ref 4c, Table I), especially the β_{11} parameter, but the positional coordinates are not inconsistent with the off-center position for K(2) in ref 3 when account is taken of experimental errors and changes of framework geometry between dK-A and dSr-A. For this new interpretation, the Sr(3)–O(1) and Sr(3)–O(2) distances of 2.96 and 2.98 ± 0.13 Å are not unusual when Sr is replaced by K; for dK-A,[3] the distances to oxygens from K(2) range upward from 2.78 ± 0.06 Å. Furthermore, partial occupancy of a site by a cation probably leads to incorrect apparent distances to neighboring oxygen atoms simply because of averaging with oxygen positions not bonded to a cation. Hence it is concluded that the concept of near-zero-coordination for Sr^{2+} is not justified by the evidence in ref 4c.

For the present structure refinements, both types of Sr atoms are near the center of a 6-ring, with Sr(1) bonded closely to three O(3) apparently at 2.41 Å and less strongly to three O(2) at 2.87 Å, and Sr(2) bonded to three O(3) apparently at 2.50 Å and less strongly to three O(2) at 2.93 Å. The shorter distances are probably too long because one-quarter of the 6-rings are unoccupied by Sr and are probably less distorted than the occupied ones.

Approximately three-quarters of the Sr atoms project into the supercage (site 1) and one-quarter into the sodalite unit (site 2). The simplest possible ionic model based merely on Sr atoms near the center of 6-rings would suggest that all Sr atoms should be in site 1 in order to maximize Sr–Sr distances. A complex model,[11] which predicted that the first five Sr^{2+} ions should go into the 6-rings[12] and the sixth into an 8-ring, is definitely inapplicable because of disagreement with the present structure determination; perhaps it is significant that the incorrect structure determination of ref 4c was then thought to be correct. Theoretical modeling to explain known data is notorious for being less convincing than successful experimental confirmation of a previous theoretical prediction. For this reason, we emphasize our own caution in attempting to explain the present observed distribution, but in a later paper we shall consider how occupancy of the Sr(2) position may be related to the presence of excess Si over the ideal Si/Al ratio of unity. To further emphasize problems in interpretation, the present data show that a simple percolation theory[13] cannot be transferred from the Ca-A to the Sr-A system, and indeed we shall present evidence that it does not even apply to Ca-A (paper in preparation).

Aluminum–Oxygen Complex. A peak of electron density at the center of the sodalite unit has been observed in the following dehydrated (d) structures: dCa-X[14] (3.4 e/Å^3); dMn-A[15] (2.3); dCo-A[16] (2.8); dCo-A·4CO[16] (1.5); dCo-A·C_2H_4[17] (4.0; also peak of 1.0 e/Å^3 at $x = y = z = 0.07$); dMn-A·C_2H_2[18] (3.4); dCo-A·C_2H_2[18] (2.3); dZn_5K_2-A[19] (2.2); dCd-A[20] (1.4); dCd-A[21] (8.2

(8) Smith, J. V.; Pluth, J. J. *Nature (London)* **1981**, *291*, 265.
(9) Cheetham, A. K.; Fyfe, C. A.; Smith, J. V.; Thomas, J. M. *J. Chem. Soc., Chem. Commun.* **1982**, 823–825.
(10) Smith, J. V. "Feldspar Minerals"; Springer: Heidelberg, 1975.
(11) Ogawa, K.; Nitta, M.; Aomura, K. *J. Phys. Chem.* **1979**, *83*, 1235–1236.
(12) Ogawa, K.; Nitta, M.; Aomura, K. *J. Phys. Chem.* **1979**, *82*, 1655–1660.
(13) Takaishi, T.; Yatsurugi, Y.; Yusa, A.; Kuratomi, T. *J. Chem. Soc., Faraday Trans. 1* **1975**, *71*, 97–105.
(14) Pluth, J. J.; Smith, J. V. *Mater. Res. Bull.* **1972**, *7*, 1311–1322.
(15) Yanagida, R. Y.; Vance, T. B.; Seff, K. *Inorg. Chem.* **1974**, *13*, 723–727.
(16) Riley, P. E.; Seff, K. *Inorg. Chem.* **1974**, *13*, 1355–1360.
(17) Riley, P. E.; Kunz, K. B.; Seff, K. *J. Am. Chem. Soc.* **1975**, *97*, 537–542.
(18) Riley, P. E.; Seff, K. *Inorg. Chem.* **1975**, *14*, 714–721.
(19) Raghavan, N. V.; Seff, K. *J. Phys. Chem.* **1976**, *80*, 2133–2137.
(20) McCusker, L. B.; Seff, K. *J. Am. Chem. Soc.* **1979**, *101*, 5235–5239.

Table II. Atomic Populations, Positions, and Displacements of Dehydrated Sr-Exchanged Zeolite A[a]

	PSfa		PSfb		PSpa	PSpb	FSp
			T				
position	96 (i)	96 (i)	96 (i)	96 (i)	24 (k)	24 (k)	24 (k)
population	96	96	96	96	24	24	24
x	0	0	0	0	0	0	0
y	0.09273 (8)	0.18847 (7)	0.09290 (15)	0.18854 (15)	0.18428 (8)	0.18428 (10)	0.1832 (4)
z	0.18590 (7)	0.09149 (9)	0.18598 (14)	0.09131 (17)	0.37423 (8)	0.37438 (10)	0.3733 (3)
β_{11}	6.4 (3)	7.3 (4)	6.3 (7)	7.2 (7)	27.2 (8)	26.8 (9)	25 (4)
β_{22}	5.7 (3)	5.6 (3)	5.4 (6)	5.7 (7)	23.4 (7)	22.9 (8)	20 (3)
β_{33}	5.2 (3)	6.0 (4)	5.0 (6)	5.8 (7)	22.7 (8)	22.5 (9)	11 (3)
β_{12}, β_{13}	0	0	0	0	0	0	0
β_{23}	0.5 (2)	0.8 (3)	0.5 (5)	1.0 (5)	1.9 (5)	2.0 (7)	1 (3)
			Sr(1)				
position	64 (g)		64 (g)		8 (g)	8 (g)	8 (g)
population	36.3 (2)		36.2 (3)		4.54 (3)	4.53 (5)	3
x, y, z	0.10434 (5)		0.10467 (8)		0.20867 (12)	0.2093 (17)	0.2050 (6)
$\beta_{11}, \beta_{22}, \beta_{33}$	16.4 (2)		16.0 (3)		65.5 (10)	63.8 (13)	63 (5)
$\beta_{12}, \beta_{13}, \beta_{23}$	9.0 (2)		8.2 (3)		36.1 (9)	33.0 (12)	49 (7)
			Sr(2)				
position	64 (g)		64 (g)		8 (g)	8 (g)	8 (g)
population	9.1 (2)		10.4 (3)		1.13 (3)	1.30 (4)	2
x, y, z	0.0747 (2)		0.0768 (3)		0.1493 (6)	0.1535 (7)	0.1550 (10)
$\beta_{11}, \beta_{22}, \beta_{33}$	19.6 (11)		17.3 (12)		78 (5)	69 (5)	73 (8)
$\beta_{12}, \beta_{13}, \beta_{23}$	13.8 (10)		12.3 (12)		55 (5)	49 (5)	28 (10)
			Al*				
position	8 (b)		8 (b)		1 (a)	1 (a)	1 (a)
population	0.44 (16)		1.5 (2)		0.05 (2)	0.18 (3)	
x, y, z	0		0		0	0	
B	0.8 (20)		2.9 (11)		0.7 (23)	2.9 (12)	
			O*				
position	64 (g)		64 (g)		8 (g)	8 (g)	8 (g)
population	1.76		6.0		0.20	0.72	
x, y, z	0.0407		0.0407		0.0814	0.0814	
B	1.2 (17)		20 (7)		0.7 (21)	20 (7)	
			O(1)				
position	96 (i)		96 (i)		12 (h)	12 (h)	12 (h)
population	96		96		12	12	12
x	0		0		0	0	0
y	0.11415 (14)		0.1142 (2)		0.2282 (3)	0.2284 (4)	0.2242 (13)
z	0.24624 (23)		0.2462 (5)		0.5	0.5	0.5
β_{11}	16.4 (8)		15.4 (9)		65 (3)	61 (4)	70 (17)
β_{22}	10.8 (6)		9.9 (8)		43 (3)	40 (4)	21 (17)
β_{33}	5.8 (7)		5.8 (11)		35 (3)	35 (3)	58 (17)
β_{12}, β_{13}	0		0		0	0	0
β_{23}	−0.4 (8)		−0.0 (15)		0	0	0
			O(2)				
position	96 (i)		96 (i)		12 (i)	12 (i)	12 (i)
population	96		96		12	12	12
x	0		0		0	0	0
y	0.13974 (20)		0.1395 (4)		0.2813 (2)	0.2810 (3)	0.2845 (9)
z	0.14160 (20)		0.1415 (4)		x	x	x
β_{11}	23.9 (9)		23.4 (11)		95 (4)	94 (5)	49 (15)
β_{22}	8.9 (11)		8.3 (24)		34 (2)	32 (2)	22 (7)
β_{33}	7.9 (11)		7.5 (24)		β_{22}	β_{22}	β_{22}
β_{12}, β_{13}	0		0		0	0	0
β_{23}	3.0 (5)		2.5 (7)		11 (2)	9 (3)	15 (11)
			O(3)				
position	192 (j)		192 (j)		24 (m)	24 (m)	24 (m)
population	192		192		24	24	24
x	0.05341 (14)		0.0532 (3)		0.1108 (2)	0.1106 (2)	0.1146 (5)
y	0.05740 (15)		0.0573 (3)		x	x	x
z	0.17294 (10)		0.1731 (2)		0.3459 (2)	0.3464 (2)	0.3459 (9)
β_{11}	11.2 (8)		12.1 (14)		47 (2)	45 (2)	24 (5)
β_{22}	10.7 (7)		8.9 (12)		β_{11}	β_{11}	β_{11}
β_{33}	12.7 (5)		11.6 (6)		51 (2)	46 (2)	48 (9)
β_{12}	4.2 (4)		4.3 (6)		14 (2)	14 (2)	13 (8)
β_{13}	1.9 (6)		1.8 (9)		7 (1)	4 (2)	10 (6)
β_{23}	1.4 (5)		0.0 (9)		β_{13}	β_{13}	β_{13}

[a] Estimated standard deviations given in parentheses to the same significance level as parameters. x, y, z given as decimal fraction of cell edge. Isotropic B given in Å^2. Anisotropic displacement factor given as $10^4 \exp[-\Sigma_{j=1}{}^{3}\Sigma_{i=1}{}^{3}\beta_{ij}h_ih_j]$.

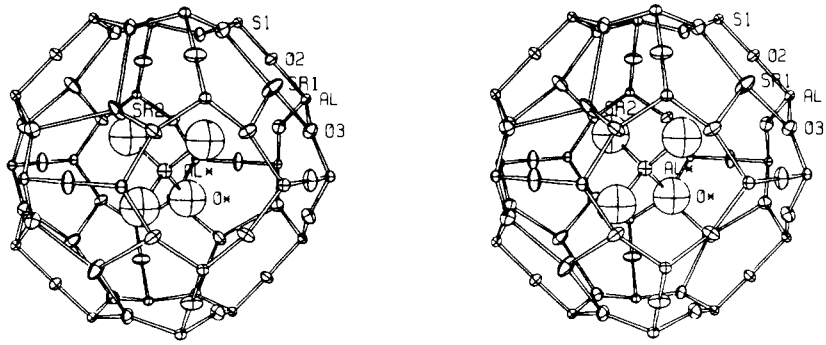

Figure 3. Stereoplot of sodalite unit and one of the AlO_4* tetrahedral units. Invert through the center of obtain the second orientation. Ellipsoids at 30% probability level.

Table III. Interatomic Distances (Å) and Angles (deg) of Dehydrated Sr-Exchanged Zeolite A

	PSfa		PSfb				
	Si	Al	Si	Al	PSpa	PSpb	FSp
T-O(1)	1.580 (6)	1.705 (6)	1.577 (12)	1.707 (12)	1.644 (2)	1.644 (2)	1.640 (6)
T-O(2)	1.594 (6)	1.725 (6)	1.589 (13)	1.734 (13)	1.657 (1)	1.660 (1)	1.659 (4)
T-2(O(3))	1.612 (4)	1.742 (4)	1.612 (9)	1.741 (9)	1.677 (1)	1.677 (1)	1.679 (4)
mean	1.600	1.728	1.598	1.731	1.664	1.664	1.644
O(1)-T-O(2)	113.8 (2)	115.1 (2)	114.2 (3)	115.0 (4)	114.5 (2)	114.6 (2)	113.3 (8)
O(1)-T-O(3)	111.6 (1)	112.6 (1)	111.6 (2)	112.7 (2)	112.0 (1)	112.0 (1)	110.2 (5)
O(2)-T-O(3)	104.9 (1)	103.5 (1)	105.0 (2)	103.5 (2)	104.3 (1)	104.3 (1)	104.2 (5)
O(3)-T-O(3)	109.7 (2)	108.7 (2)	109.2 (3)	108.7 (3)	109.2 (2)	109.1 (2)	114.4 (5)
T-O(1)-T	141.3 (2)		141.1 (3)		141.5 (3)	141.3 (3)	144 (1)
T-O(2)-T	177.5 (3)		178.0 (3)		177.5 (3)	178.0 (3)	172 (1)
T-O(3)-T	146.8 (2)		147.2 (2)		146.9 (2)	147.2 (2)	143.6 (8)
Sr(1)-3(O(3))	2.405 (3)		2.416 (3)		2.405 (3)	2.415 (3)	2.343 (9)
Sr(1)-3(O(2))	2.870 (2)		2.871 (2)		2.870 (2)	2.871 (2)	2.880
Sr(1)-O*	2.719 (2)		2.736 (4)		2.719 (3)	2.736 (4)	
Sr(2)-3(O(3))	2.517 (4)		2.495 (5)		2.517 (5)	2.496 (5)	2.454 (12)
Sr(2)-3(O(2))	2.949 (4)		2.923 (5)		2.949 (5)	2.923 (5)	2.955

± 3.8 e/Å^3 for dehydration at 600 °C and 4.5 ± 3.8 e/Å^3 for 700 °C); dZn-A[22] (4.9 ± 0.6 e/Å^3). Because corresponding structures involving monovalent ions do not show a peak at the center of the sodalite unit, it is certain that the peak in these structures with divalent ions is not just an artifact of the mathematical procedure of least-squares refinement.

Two possibilities were considered: (a) an oxygen species obtained by dissociation of water during dehydration (e.g., ref 22 and 23), and (b) some kind of species obtained by dissociation of the aluminosilicate framework. The former possibility does not explain the peak near ±0.08, ±0.08, ±0.08 (pseudocell) on the eight triad axes, and it does not provide a suitable bonding distance to either the aluminosilicate framework or the Sr atoms. The second possibility is viable because the eight peaks on the triad axes can be split up into two sets of four peaks, each of which corresponds to the vertices of a tetrahedron. One set is shown in Figure 2, and the other set can be obtained by inversion through a center of symmetry. Furthermore, the interatomic distances, although not well-defined (Figure 2), are consistent with expected values for a tetrahedron TO_4. An octahedral complex can be ruled out because the electron density peaks for its O species should lie along cubic [100] rather than tetrahedral [111] directions.

It is not possible to identify the type of tetrahedral complex from the present data because of the low accuracy of position of electron-density contours (Figure 2) and the closeness of expected T–O distances. The TO_4 complex might be uncharged with composition $(Al_xSi_{1-x})O_4H_x$ or charged with composition $(Al_xSi_{1-x})O_4^{x-}$. Expected distances are approximately 1.60 Å (Si–O), 1.65 Å (Si–OH), 1.74 Å (Al–O), 1.80 Å (Al–OH), and the observed electron densities for crystal PSb in Figure 2 are consistent with the assumed distance of 1.74 Å for Al–O but do not exclude the other species. The noncircularity of the peaks for O* in Figure 2 may indicate some angular misorientation of the presumed TO_4 tetrahedra, and this might be the result of interaction with framework oxygens and strontium atoms. It will now be assumed that the extra electron density belongs to an AlO_4 rather than an SiO_4 species merely because there is considerable evidence[24] for removal of Al from zeolite frameworks by various process. Furthermore, the sum total of evidence on aluminosilicate frameworks indicates that Si-rich tetrahedral frameworks tend to be more stable than Al-rich frameworks, in part because Al has a considerable tendency to go into an octahedral environment.

It should be emphasized that the absence of X-ray evidence for an occluded AlO_4 species in *monovalent* varieties of zeolite A implies that the occluded AlO_4 species in the *divalent* varieties developed during ion exchange with divalent cations or during subsequent dehydration, or both. Hence, the NMR evidence[6] for occluded aluminum compounds in as-synthesized A zeolites does not apply to the specimens exchanged with divalent cations. Apparently the lack of detectable peaks of electron density for the monovalent varieties of zeolite A implies that the occluded aluminum compounds detected in ref 6 are at a rather low concentration.

Because of the small population factors for the Al* and O* positions and the incomplete site occupancy for Sr(1) and Sr(2), the following discussion is speculative. Each O* site lies at 3.3 Å to the three nearest framework oxygens of type O(3) and at 2.72 Å to an Sr(1) site along the same body diagonal (Figure 3). Small atomic displacements might change these distances to ex-

(21) McCusker, L. B.; Seff, K. *J. Phys. Chem.* **1980**, *84*, 2827–2831.
(22) McCusker L. B.; Seff, K. *J. Phys. Chem.* **1981**, *85*, 405–410.
(23) Bennett, J. M.; Smith, J. V. *Mater. Res. Bull.* **1969**, *4*, 77–86.
(24) McDaniel, C. V.; Maher, P. K. *ACS Monogr.* **1976**, No. *171*, 285–331.
(25) In addition to local programs for data reduction, local variations of the following programs were used in this study: FORDAP Fourier programs of A. Zalkin; NUCLS, a least-squares program resembling Busing-Levy ORFLS; ORFFE error function program of W. R. Busing and N. A. Levy; and ORTEP, a plotting program by C. Johnson.

pected bonding values of about 2.8–3.0 Å, respectively. Indeed, the noncircularity of the electron-density peaks for O* in Figure 2 might result from such displacements. Distances to Sr(2) are either too short (1.48 Å) or too long (<3 Å), and there is no reason to associate an AlO_4* complex with the displacement of this type of Sr atom into the sodalite unit rather than into the large cage.

Acknowledgment. This work was supported primarily by National Science Foundation Grant CHE 80-24138 and secondarily by the Materials Research Laboratory funded by NSF Grant 79-24007. We acknowledge financial support from Union Carbide Corp. given in memory of Donald W. Breck. We thank I. M. Steele, N. Weber, and O. Draughn for technical help, and G. T. Kokotailo for material assistance.

Supplementary Material Available: A listing (Table IV) of the observed and calculated structure factors (7 pages). Ordering information is given on any current masthead page.

Mixed-Valence Semiquinone–Catecholate–Iron Complexes

Michael W. Lynch,[1] Mark Valentine,[2] and David N. Hendrickson*[1]

Contribution from the School of Chemical Sciences and Department of Physics, University of Illinois, Urbana, Illinois 61801. *Received December 14, 1981*

Abstract: The complex $[Fe(phenSQ)_3]\cdot phenQ$, where phenQ and phenSQ are quinone and semiquinone forms, respectively, of 9,10-phenanthrenequinone, reacts with either 2,2′-bipyridine (bpy), 1,10-phenanthroline (phen), or 5,5′-dimethyl-2,2′-bipyridine (dmbpy) to give complexes of the formulation Fe(phenSQ)(phenCAT)(bidentate nitrogen base). Iron-57 Mössbauer and magnetic susceptibility data indicate that these three complexes are high-spin iron(III) complexes. The mixed-valence character with one semiquinone and one catecholate ($phenCAT^{2-}$) ligand is substantiated by the observation of an intervalence transfer band at 1100 nm in the solid state and in low dielectric constant solvents. In high dielectric solvents there is no IT band and other features are changed, suggesting an *intramolecular* electron transfer to a $Fe^{II}(phenSQ)_2$(bidentate nitrogen base) species. Five analogous compounds can be prepared by the reaction of $Fe(DBSQ)_3$, where DBSQ is the semiquinone form of 3,5-di-*tert*-butyl-1,2-benzoquinone, with bpy, phen, dmbpy, py, and en. These five complexes have the composition Fe^{III}(DBSQ)(DBCAT)(nitrogen base) and are most likely oligomeric in the solid state. No IT bands are seen for these five complexes; however, support for the mixed-valance composition is drawn from infrared spectra.

The interaction between iron centers and quinones plays an important role in bacterial photosynthesis.[3,4] The primary photochemical event in bacterial photosynthesis is a light-induced electron transfer from a primary electron donor to a primary electron acceptor. This event occurs in a bacteriochlorophyll–protein complex called the reaction center where a special bacteriochlorophyl dimer is believed to be the primary electron donor.[5-7] The identity, composition, and mechanism of the primary electron acceptor has been more elusive and is a topic of considerable research. Presently, the primary electron acceptor is believed to a an ubiquinone (Q_I).[3,4,6] Following excitation of the reaction center by a photon, Q_I is reduced to an anionic semiquinone which has been identified by EPR.[4,9] A broad, grossly distorted EPR signal has been observed at $g \sim 1.82$ caused by a weak magnetic interaction with an adjacent iron species. The iron is found to be in the high-spin ferrous state in both the resting and reduced forms of the reaction center, as determined by magnetic susceptibility[10] and ^{57}Fe Mössbauer[11,12] measurements. The iron center is evidently very important to the action of the reaction center since in its absence electrons cannot be shuttled from Q_I to the nearby secondary acceptor quinone, Q_{II}.[13] Secondly, without the presence of iron, Q_I exhibits normal quinone chemistry and acts as a two-electron acceptor. The iron center causes the second redox potential ($Q_I^{-}\cdot/Q_I^{2-}$) to be of inaccessibly low value[14] and, therefore, has a profound influence on the one-electron shuttling behavior of Q_I. The iron–quinone complex of the reaction center may be usefully described as Q_IFeQ_{II}. The exact environment about these two quinones and about the iron is not well characterized. However, EPR and EXAFS measurements seem to suggest that each of the quinones is in a different environment and is probably not directly bonded to the iron center.[10,15] As electrons are shuttled through the reaction center, several intermediates are formed. They have been detected spectroscopically and their identities postulated to include (Q_IFeQ_{II}), ($Q_I^{-}\cdot FeQ_{II}$), ($Q_IFeQ_{II}^{-}\cdot$), and ($Q_I^{-}\cdot FeQ_{II}^{-}\cdot$).[3] The last form has proven quite interesting and elusive because the two semiquinones are apparently magnetically coupled in this state. This situation is believed to involve the iron since it is inolved in magnetic interactions with each semiquinone individually and is important in mediating the Q_I–Q_{II} electron transfer.

(1) School of Chemical Sciences.
(2) Department of Physics.
(3) Wraight, C. A. *Photochem. Photobiol.* **1979**, *30*, 767.
(4) Feher, G.; Okanura, M. Y., In "The Photosynthetic Bacteria"; Clayton, R. K.; Sistrom, W. R., Eds.; Plenum Press: New York 1978.
(5) Norris, J. R.; Uphaus, R. A.; Crespi, H. L.; Katz, J. J. *Proc. Natl. Acad. Sci. U.S.A.* **1971**, *68*, 625.
(6) Feher, G.; Hoff, A. J.; Isaacson, R. A.; Ackerson, L. C. *Ann. N.Y. Acad. Sci.* **1975**, *244*, 239.
(7) Norris, J. R.; Sheer, H.; Katz, J. J. *Ann. N.Y. Acad. Sci.* **1975**, *244*, 261.
(8) Parson, W. W.; Cogdell, R. J. *Biochim. Biophys. Acta* **1975**, *416*, 105.
(9) Dutton, P. L. *Photochem. Photobiol.* **1976**, *24*, 655. Wraight, C. A. *Biochim. Biophys. Acta* **1977**, *459*, 525. Okamura, M. Y.; Isaacson, R. A.; Feher, G. *Biophys. J.* **1978**, *21*, 8a.
(10) Butler, W. F.; Johnston, D. C.; Shore, H. B.; Fredkin, D. R.; Okamura, M. Y.; Feher, G. *Biophys. J.* **1980**, *32*, 967.
(11) Debrunner, P. G.; Smith, C. E.; Feher, G.; Okamura, M. Y. *Biophys. J.* **1975**, *15*, 226a.
(12) Boso, B.; Debrunner, P. G.; Okamura, M. Y.; Feher, G. *Biochim. Biophys. Acta* **1981**, *638*, 173.
(13) Blankenship, R. E.; Parson, W. W. *Biochim. Biophys. Acta* **1979**, *545*, 429.
(14) Dutton, P. L.; Prince, R. C.; Tiede, D. M. *Photochem. Photobiol.* **1978**, *28*, 939.
(15) Wraight, C. A. *FEBS Lett.* **1978**, *93*, 283.

0002-7863/82/1504-6982$01.25/0